18th Brazilian Congress of Thermal Sciences and Engineering
November 16-20, 2020 (Online)

ENC-2020-0203
LATTICE BOLTZMANN SIMULATION PAST A CIRCULAR CYLINDER: COMPARISON BETWEEN MODELS AND BOUNDARY CONDITIONS

Jorge Lucas Krenchiglova
Paulo Cesar Philippi
Pontifical Catholic University of Paraná – PUCPR, R. Imaculada Conceição, 1155, Prado Velho, Curitiba, PR, Brazil.
e-mails: jorge.l.krenchiglova@outlook.com, philippi@lmpt.ufsc.br

Luís Orlando Emerich dos Santos
Universidade Federal de Santa Catarina – UFSC, R. Presidente Prudente de Moraes, 406, Santo Antônio, Joinville, SC, Brazil.
e-mail: luis.emerich@ufsc.br

Abstract. *This paper presents the numerical simulation of an incompressible two-dimensional flow around a circular cylindrical obstacle for a variety of Reynolds numbers. Three different models of the Lattice Boltzmann (LB) equation are discussed: the classic kinetic model BGK, a regularized model and a model with two relaxation times, for the latter two approaches are presented and compared. Also, a large number of different boundary conditions are compared. To validate the results, the drag coefficients and the flow representation were compared with several authors in the literature. It was possible to conclude that the models presented here are very well suitable both for the estimation of the aerodynamics coefficients and for the representation of the flow.*

Keywords: *Lattice Boltzmann Method (LBM), Regularized model, Two relaxation times (TRT), Drag, Lift.*

1. INTRODUCTION

Fluid dynamics is a branch of applied science, which focus is to investigate the movement of fluids, such as liquid and gases, and how forces affect them. Sometimes, problems in fluid dynamics may prove to be very much complex and troublesome, or even impossible to be solved directly or reproduced. Due to these facts, Computational Fluid Dynamics (CFD) has been used as an alternative method to study fluid physics related phenomena. Firstly, introduced in the early 1970s, the method consists in the numerical solution of the mass, momentum, and energy conservation equations and soon it grew to become a remarkable synergy of physics, applied mathematics, and computer sciences.

The Lattice Boltzmann Method (LBM) is a particle-based approach to CFD, using microscopic models and mesoscopic kinetic equations. Indeed, the LBM has its roots in the Lattice Gas Automata (LGA). In this particular method, fictitious particles exist within a numerical domain where they stream and collide in a manner that respects the mass and momentum conservation (Kruger et al., 2017; Rothman; Zaleski, 1997; Succi, 2001). Later, McNamara and Zanetti (MZ) (McNamara; Zanetti, 1988) replace the boolean variable present in the LGA by a set of real-valued populations, soon after, Higuera and Jimenez (Higuera; Jiménez, 1989) proposed a linear approximation for the collisional operator in the MZ model, followed by (Chen et al., 1991; Qian; D'Humières; Lallemand, 1992) which introduced a simplified collisional model with a single relaxation time that has the same formulation as the BGK model (Bhatnagar; Gross; Krook, 1954) in kinetic theory, this model is called LBGK. Some years later the LB equation was recognized as a discrete form of the Boltzmann transport equation by (Abe, 1997; He; Luo, 1997; Philippi et al., 2006; Shan; Yuan; Chen, 2006).

The LBM model already had proved itself to be a very reliable tool in handling flow simulation around complex geometries and fluid-solid interaction as pointed by several authors (Chen; Doolen, 1998; Higuera; Succi, 1989). The flow around bluff bodies is a permanent subject of interest due to its increasing complexity with the Reynolds number (*Re*). The flow pattern for a single circular cylinder with *Re* ranging between $Re \approx 5$ *and* 40 the flow remains stable and a pair of vortices appear behind the solid body; these vortices increase in size as Re increases until reaching a critical limit. At this limit, when *Re* is greater than *~45*, the vortices began to shed off and the flow becomes unstable, at this moment it is observed the formation of the Von Kármán vortex streets. (Dennis; Chang, 1970; Fornberg, 1980; Surmas; Dos Santos; Philippi, 2004).

This work is restricted to a two-dimensional incompressible flow around a circular cylinder obstacle with a set of Reynolds numbers ranging from $Re = 10$ until 100. We deal with different models of the LBGK algorithm and investigate a variety of boundary conditions. Also, we study the behavior of the aerodynamic forces using the momentum exchange method (MEM).

2. THE LBGK MODEL

As previously mentioned, a LB equation may be seen as a first-order, finite-difference numerical approximation of the continuous Boltzmann transport equation. So, let $f_i(\boldsymbol{x}, \boldsymbol{e}_i, t)$ be a dimensionless pack of particles traveling with the dimensionless discrete velocity $\boldsymbol{e}_i$ and found on site $\boldsymbol{x}$ at time t. Using the single relaxation time BGK collision model (Chen et al., 1991; Qian; D'Humières; Lallemand, 1992):

$$f_i\left(\mathbf{x}+\mathbf{e}_i h, t+\delta\right) = f_i\left(\mathbf{x}, t\right) + \frac{f_i^{eq} - f_i}{\tau^*} \tag{1}$$

where τ^* is a dimensionless relaxation time, which is related to the fluid kinematic viscosity in accordance with $\nu = \frac{h^2}{\delta} c_s^2(\tau^* - 1/2)$, c_s is the sound speed for a given discrete representation, δ is the time step and h is the orthogonal distance between any two contiguous sites. Function f_i^{eq} is a polynomial approximation to the Maxwell-Boltzmann (MB) equilibrium distribution function, which, in present case, can be written as a second-order Hermitian polynomial expansion (Philippi et al., 2006),

$$f_i^{eq} = \rho W_i\left[1+\mathbf{u}_\alpha \mathbf{e}_{i\alpha} + \left(1/2!\right)\mathbf{u}_\alpha \mathbf{u}_\beta\left(\mathbf{e}_{i\alpha}\mathbf{e}_{i\beta} - c_s^2\delta_{\alpha\beta}\right)\right], \tag{2}$$

where $\delta_{\alpha\beta}$ is the Kronecker delta, W_i are weighting factors for the lattice scheme, which for a D2Q9 two-dimensional 9-velocity vectors lattice, (Philippi et al., 2006) are given in Tab. 1.

Table 1. Lattice-Boltzmann parameters for the D2Q9 lattice. The sound speed in this lattice is $c_s = 1/\sqrt{3}$.

i	$\boldsymbol{e}_i$	W_i
0	$(0,0)$	$16/36$
$1-4$	$(\pm1,0),(0,\pm1)$	$4/36$
$5-8$	$(\pm1,\pm1)$	$1/36$

Also,

$$\rho = \sum_i f_i \quad \rho\mathbf{u}_\alpha = \sum_i f_i \mathbf{e}_{i\alpha}\ , \tag{3}$$

are the local mass density and momentum, respectively.

3. MODEL IMPROVEMENTS

The most commonly used lattice Boltzmann collision model is the single relaxation-time BGK model (Bhatnagar; Gross; Krook, 1954). This model is able to asymptotically represent near incompressible flows. Nevertheless, it suffers from instability drawbacks especially at high Reynolds numbers. In the following, we present two methods that have been developed to soften these instability issues, enlarging the stability range of LB algorithms.

3.1 Regularization

Regularization is a common procedure in CFD methods to smooth the errors carried throughout the simulation. In LBM, the regularization method is a way of filtering out those errors produced by non-hydrodynamic high-order non-equilibrium moments. (Mattila; Philippi; Hegele, 2017; Zhang; Shan; Chen, 2006).

The LBGK model, Eq. (1), can be rewritten in its regularized (RLBGK) form as:

$$f_i\left(\mathbf{x}+\mathbf{e}_i\delta, t+\delta\right) = f_i^{eq}\left(\mathbf{x}, \mathbf{e}_i, t\right) + \left(1-\omega\right)\hat{f}_i^{neq}\left(\mathbf{x}, \mathbf{e}_i, t\right), \tag{4}$$

where ω is the relaxation frequency defined by $\omega = \delta/\tau$ and $\hat{f}_i^{neq}$ is the regularized, non-equilibrium part of the distribution function $f_i = f_i^{eq} + \hat{f}_i^{neq}$, which can be expanded into a Hermitian polynomial expansion. The first two

zeroth and first-order moments, of the Hermitian expansion correspond, respectively, to the contribution of the non-equilibrium distribution to the conservation of mass and momentum, so it is equal zero, thus summarizing to a second-order expansion: (Mattila; Philippi; Hegele, 2017)

$$\hat{f}_i^{neq} = W_i\left[\left(1/2!cs^4\right)\tau_{\alpha\beta}\left(\mathbf{e}_{i\alpha}\mathbf{e}_{i\beta} - c_s^2\delta_{\alpha\beta}\right)\right], \tag{5}$$

where $\tau_{\alpha\beta}$ is the viscous stress tensor.

3.2 Two Relaxation Times (TRT)

The BGK collision operator produces second-order Knudsen errors. To soften these errors, (Ginzburg; Verhaeghe; D'Humières, 2008) proposed a model based on two relaxation times; the first of them is related to viscosity and the second one is a free parameter. In this model, the populations are decomposed into a symmetric and anti-symmetric part as shown:

$$f_i^e = (1/2)\left(f_{i^+} + f_{i^-}\right) \quad f_i^o = (1/2)\left(f_{i^+} - f_{i^-}\right), \tag{6}$$

where the e and o symbols denote the symmetrical and anti-symmetrical parts respectively, also the $f_{i^+} = f_i(e_i)$ designates the populations along the e_i directions and $f_{i^-} = f_i(-e_i)$ is the populations along the $-e_i$ directions. With this in mind, the LBGK model, Eq. (1), may be rewritten as

$$f_i\left(\mathbf{x}+\mathbf{e}_i\delta, t+\delta\right) - f_i\left(\mathbf{x},t\right) = \frac{\delta}{2\tau_e}\left[\left(f_{i^+}^{eq} + f_{i^-}^{eq}\right) - \left(f_{i^+} + f_{i^-}\right)\right] + \frac{\delta}{2\tau_o}\left[\left(f_{i^+}^{eq} - f_{i^-}^{eq}\right) - \left(f_{i^+} - f_{i^-}\right)\right], \tag{7}$$

where the even τ_e and odd τ_o relaxation times are, respectively, related to the symmetric and anti-symmetric parts of the populations. The even part (τ_e) is related to the viscosity and the odd part (τ_o) is dependent on τ_e. (Philippi, 2018) presents the following relationship for the dimensionless relaxation times $\tau_e^* = \tau_e/\delta$ and $\tau_o^* = \tau_o/\delta$:

$$\tau_o^* = \frac{\tau_e^* - (1/3)}{2\tau_e^* - 1}, \tag{8}$$

although (Luo et al., 2011) presents a different relationship:

$$\tau_o^* = \frac{\tau_e^* - (1/8)}{2\tau_e^* - 1}. \tag{9}$$

4. BOUNDARY CONDITIONS

4.1 Fluid-solid interaction

The half-way bounce back (HWBB) boundary condition is the most frequently used boundary condition in LBM, for imposing the fluid-solid adherence at the solid external surface. It is very simple to implement, especially in complex geometry and credited to have second-order accuracy.

It can be written for all boundary sites $\mathbf{x}_b$ next to the solid surface (Figure 1), as:

$$f_{-i}\left(\mathbf{x}_b, t+\delta\right) = f_i\left(\mathbf{x}_b, t\right) \tag{10}$$

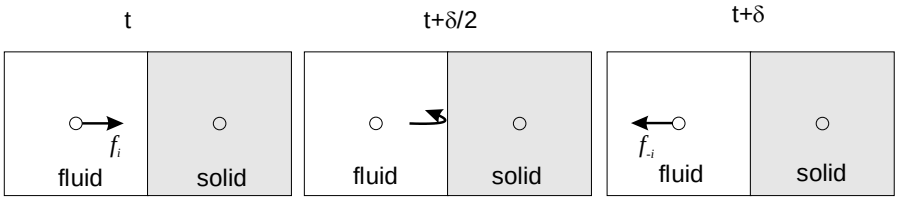

Figure 1. Half-way bounce back boundary condition.

where symbol i denotes a direction pointing to the solid.

4.2 Boundary conditions for the frontiers of the computational domain

Six kinds of boundary conditions were used for the frontiers of the computational domain: Zou & He, periodic, free-slip, full developed, pressure imposed and regularized.

4.2.1 Entrance nodes

For the entrance of the computational domain we ascribe a uniform velocity profile $u_x = u_0$, $u_y = 0$ for all nodes $(0, y)$.

Zou and He (Zou; He, 1997) proposed a BC model (ZH) based on the bounce-back of the non-equilibrium populations along the normal directions to the boundary. This *Ad-Hoc* assumption:

$$f_1^{neq} = f_3^{neq}, \tag{11}$$

provides the fourth equation that is needed for solving the hydrodynamic equations for ρ, f_1, f_5, f_8 at the boundary in Figure 2, in addition to:

$$\sum_i f_i = \rho, \quad \sum_i f_i \mathbf{e}_{ix} = \rho \mathbf{u}_0, \quad \sum_i f_i \mathbf{e}_{iy} = 0, \tag{12}$$

when the macroscopic velocity is known at the entrance of the numerical domain $u_x = u_0$, $u_y = 0$ for all nodes $(0, y)$.

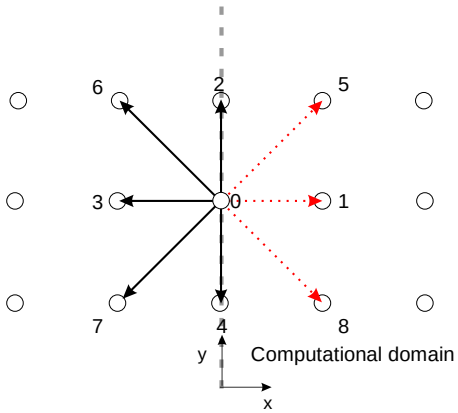

Figure 2. Unknown populations f_1, f_5, f_8 in a node at the entrance of the numerical domain.

For the regularized model the boundary conditions follow the model proposed by (Hegele et al., 2018). Second-order moments are required to satisfy.

$$\tau_{\alpha\beta} = \sum_{i \in I} f_i \mathbf{e}_{i\alpha} \mathbf{e}_{i\beta} - \sum_{i \in I} f_i^{eq}(\rho) \mathbf{e}_{i\alpha} \mathbf{e}_{i\beta} + \sum_{i \notin I} \hat{f}_i^{neq}(\tau_{xx}, \tau_{xy}, \tau_{yy}) \mathbf{e}_{i\alpha} \mathbf{e}_{i\beta}, \tag{13}$$

where $I = \{0,2,3,4,6,7\}$ is the set of incoming directions from the nodes of the computational domain. Since the velocity components are prescribed at the entrance nodes, a set of 4 equations for the unknowns $\rho, \tau_{xx}, \tau_{xy}, \tau_{yy}$ is then closed by requiring.

$$\sum_i f_i = \sum_{i \in I} f_i + \sum_{i \notin I} \hat{f}_i = \rho \tag{14}$$

The solution of Eqs. (13) and (14) enables to find the moments $\rho, \tau_{xx}, \tau_{xy}, \tau_{yy}$ and the unknown populations f_1, f_5, f_8.

4.2.2 Side nodes

Simulation results are very sensible to the numerical domain dimensions and to the kind of boundary conditions used. This is especially important when there is the formation of a vortex street, since the vortex streets grows laterally and extend over several cylinder diameters. From a simulation standpoint, some kind of truncation must be adopted at the lateral and end surfaces of the simulation domain.

So periodicity in present context means that, if H denotes the vertical dimension of the computational domain and at node $(x, 0)$ direction i points outside of the simulation domain, the outgoing population $f_i(x, 0)$ is transferred to the node (x, H) in accordance with:

$$f_i(x, H) = f_i(x, 0) \tag{15}$$

On the other hand, the free-slip boundary condition means that populations reaching one of the two lateral surfaces suffer a specular reflection back into the simulation domain. This BC is used when there is an undesirable transfer of information (or fields) throughout the frontier and we judge it is possible to avoid this transfer.

4.2.3 Exit nodes

Full developed BC condition means that the simulation domain extension L along the *x*-coordinate is large enough in such a way that there is no more variation of the particle populations with x at $x = L$. It is of common practice to repeat the data for nodes $(L - 1, y)$ attributing this data to the nodes (L, y).

Another alternative is to ascribe the pressure at $x = L$.

5. RESULTS AND DISCUSSION

The numerical simulations were carried out for a set of Reynolds numbers of $Re = 10, 20, 40$ e 100; the dimensions of the numerical domain used for the study were 1200×1000 sites, with 40 sites in the diameter (d) of the circular cylinder and with its center located $7.5d$ sites of distance from the domain entrance, as shown in Fig. 1.

The Reynolds number was taken as:

$$\mathrm{Re} = \frac{u_0 d}{c_s^2 \left(\tau^* - 1/2\right)}, \tag{16}$$

where u_0 is the dimensionless uniform velocity at the entrance of the numerical domain, d is the cylinder diameter in lattice unities and $\tau^* = \tau/\delta$ is the dimensionless relaxation time. For avoiding compressibility effects and third order errors in the Navier-Stokes equations, the velocity u_0 was kept at a very low value $u_0 = 0.04$.

The studies were performed for the LBGK and RLBGK models with a single relaxation time (SRT), in addition to this, tests with the TRT model were carried out with the relationship Eq. (8) presented by (Philippi, 2018) and also the relationship Eq. (9) presented by (Luo et al., 2011). The boundary conditions used are described as follows: uniform speed at the domain entrance, pressure conditions at the exit, periodic and free-sleep conditions at the upper and lower boundary, and for the fluid-solid interaction the halfway bounce back was used.

For the LBGK models:

- **Case A: entrance:** Zou and He (Zou; He, 1997) boundary conditions; **exit:** full developed; **upper and lower ends:** periodic condition;
- **Case B: entrance:** Zou and He (Zou; He, 1997) boundary conditions; **exit:** full developed; **upper and lower ends:** free-slip condition;

- **Case C: entrance:** Zou and He (Zou; He, 1997) boundary conditions; **exit:** ascribed pressure; **upper and lower ends:** periodic condition;
- **Case D: entrance:** Zou and He (Zou; He, 1997) boundary conditions; **exit:** ascribed pressure; **upper and lower ends:** free-slip condition.

For the RLBGK models:

- **Case A: entrance:** regularized boundary conditions (Hegele et al., 2018); **exit:** full developed; **upper and lower ends:** periodic condition;
- **Case B: entrance:** regularized boundary conditions (Hegele et al., 2018); **exit:** full developed; **upper and lower ends:** free-slip condition;
- **Case C: entrance:** regularized boundary conditions (Hegele et al., 2018); **exit:** ascribed pressure; **upper and lower ends:** periodic condition;
- **Case D: entrance:** regularized boundary conditions (Hegele et al., 2018); **exit:** ascribed pressure; **upper and lower ends:** free-slip condition.

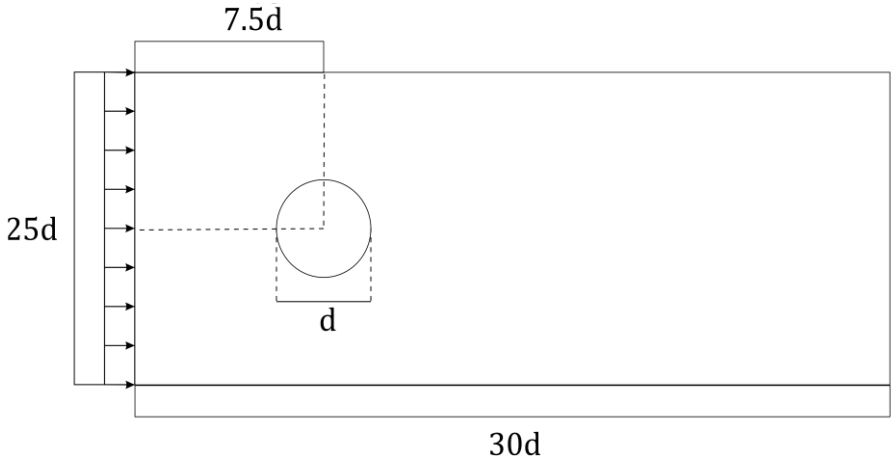

Figure 3. Computational domain and solid body.

Figure 4 shows the streamlines of the flow past the cylinder for three different Reynolds obtained for case A. At $Re = 20$ and $Re = 40$, the flow separates on the downstream side, and two steady standing vortices are formed. These vortices are stable and remain attached to the body.

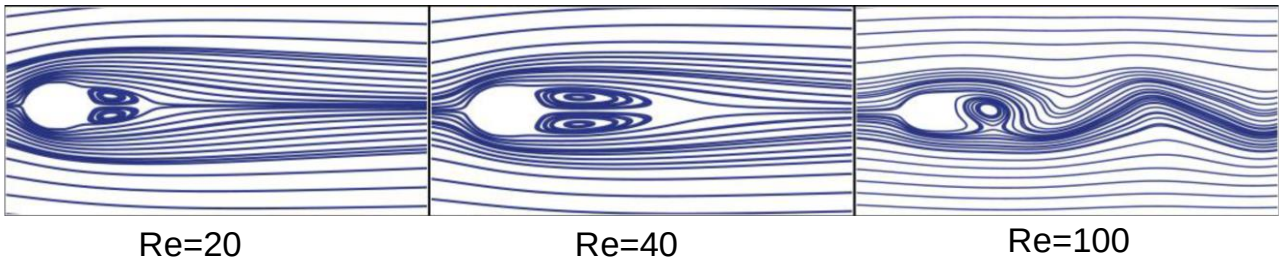

Figure 4. Streamlines of the flow behind the cylinder section for $Re = 20$, 40 and 100. Simulations were performed with LBGK (case A).

When the Reynolds number grows beyond 40, a new flow pattern develops. The wake behind the cylinder become unstable. Oscillations in the wake grow in amplitude and finally roll up into discrete vortices with a very regular spacing. This trail of vortices in the wake is known as the von Karman vortex street. This vortex releasing is shown in Figure 4 for $Re = 100$.

Vortex formation near the cylinder is an unsteady flow, and the drag force oscillates with the formation of each eddy. In present simulations these vortices are released from the cylinder after about 40000 time steps. In addition, the top-to-bottom asymmetry of the flow gives rise to an oscillating lift force. As the flow forms a clockwise eddy, it rushes past the top of the cylinder somewhat faster than the flow across the bottom. This causes the pressure on the top to be less, resulting in a lift force toward the top. When the clockwise eddy breaks away, the opposite pattern develops on the bottom and the lift force reverses its direction. This is clearly shown in Figure 5 (right).

Table 2 shows a comparison between the results obtained for the drag coefficient using the BGK and the RBGK regularized version. As it was to be expected, in this range of Reynolds number, there are no meaningful differences

between the results obtained using these two methods. Indeed, high-order ghost moments manifestation is only expected for higher Reynolds number and their effect is to produce instability in the numerical scheme. Therefore, these effects can be only appreciated for intermediate and high values of the Reynolds number.

In the same manner, as shown in Tab. 3, in this range of Reynolds number, simulations appear to be insensible to the particular relationship between the odd and the even relaxation times found by different authors for avoiding the influence of second-order Knudsen errors.

Nevertheless, if the simulation results appear to be insensible to the method in this range of Reynolds number, they are very sensible to the numerical domain dimensions and to the kind of boundary conditions used. This is a crucial question when the vortices are detached from the cylinder surface since the vortex streets grows laterally and extend over several cylinder diameters. From a simulation standpoint, some kind of truncation must be adopted at the ends of the numerical simulation domain.

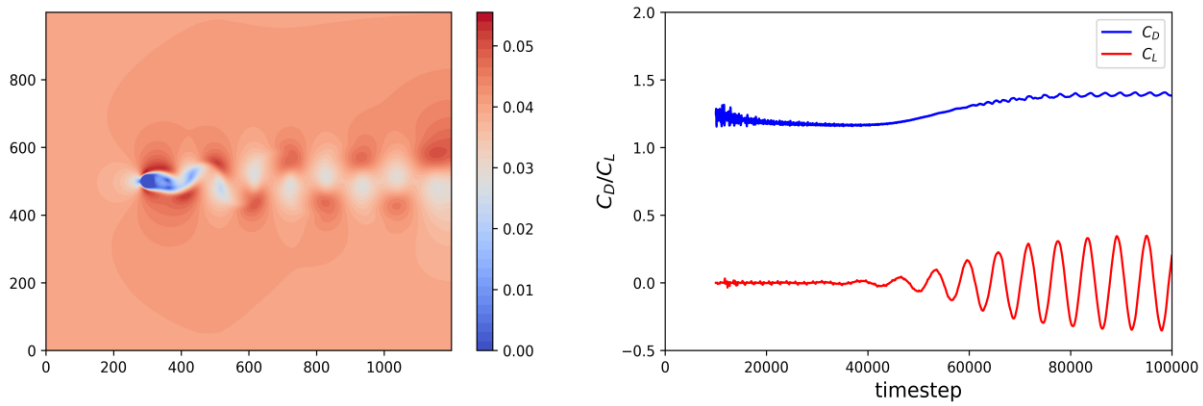

Figure 5. Left: velocity field representation; Right: aerodynamic coefficients temporal progression; Both images for the simulations performed with RBGK, case A and $Re = 100$.

Table 2. Comparisons for the drag coefficient obtained for the BGK and RBGK simulations.

		Drag coefficient C_D			
Reynolds number		10	20	40	100
BGK	A	3.072	2.195	1.631	1.398
	B	3.076	2.201	1.642	-
	C	3.080	2.201	1.639	1.396
	D	3.080	2.201	1.639	1.397
RBGK	A	3.076	2.200	1.640	1.398
	B	3.076	2.200	1.640	-
	C	3.080	2.200	1.638	1.398
	D	3.080	2.200	1.638	1.399

Table 3. Comparisons for the drag coefficient obtained for the BGK-TRT simulations.

		Drag coefficient C_D			
Reynolds number		10	20	40	100
TRT with Eq. (8)	A	3.079	2.200	1.639	1.394
	B	3.079	2.200	1.639	-
	C	3.083	2.201	1.637	1.393
	D	3.083	2.201	1.637	1.393
TRT with Eq. (9)	A	3.077	2.198	1.638	1.392
	B	3.077	2.198	1.638	-
	C	3.081	2.199	1.635	1.389
	D	3.081	2.199	1.635	1.391

Figure 6 shows a comparison between the sets of boundary conditions used for the LBGK simulation. In case A periodic conditions were used for the upper and lower ends of the numerical domain and this is the only difference when case A is compared with case B, for which a free-slip boundary condition was used. It is apparent that while the periodic conditions give rise to steady temporal profiles of the drag and lift coefficients after 100000 time steps, the use of a free-

slip boundary condition requires a larger number of time steps to converge to a steady drag profile. In addition, the lift coefficient oscillates with a larger amplitude: 0.55 against 0.35, in the former case.

While periodic conditions mean that the populations arriving at one of the sides are transferred to the other side, free slip means that these populations are reflected back with a specular reflection. Both conditions are suitable for the problem when the numerical domain is large enough and this difference although difficult to explain, mean that some information of the vortex street is touching the upper and lower sides of the numerical domain.

Case A is now compared with cases C and D, for which the pressure was imposed at the right end of the numerical domain. Since the imposed pressure results different from the one that is propagated from the left, this imposition produces a finite pressure perturbation that is reflected back into the numerical domain as an acoustic wave and is responsible for a very noisy profile for the drag and lift coefficients (Figure 6). Nonetheless, both the average value for the drag coefficient and the amplitude of the lift are in agreement with case A.

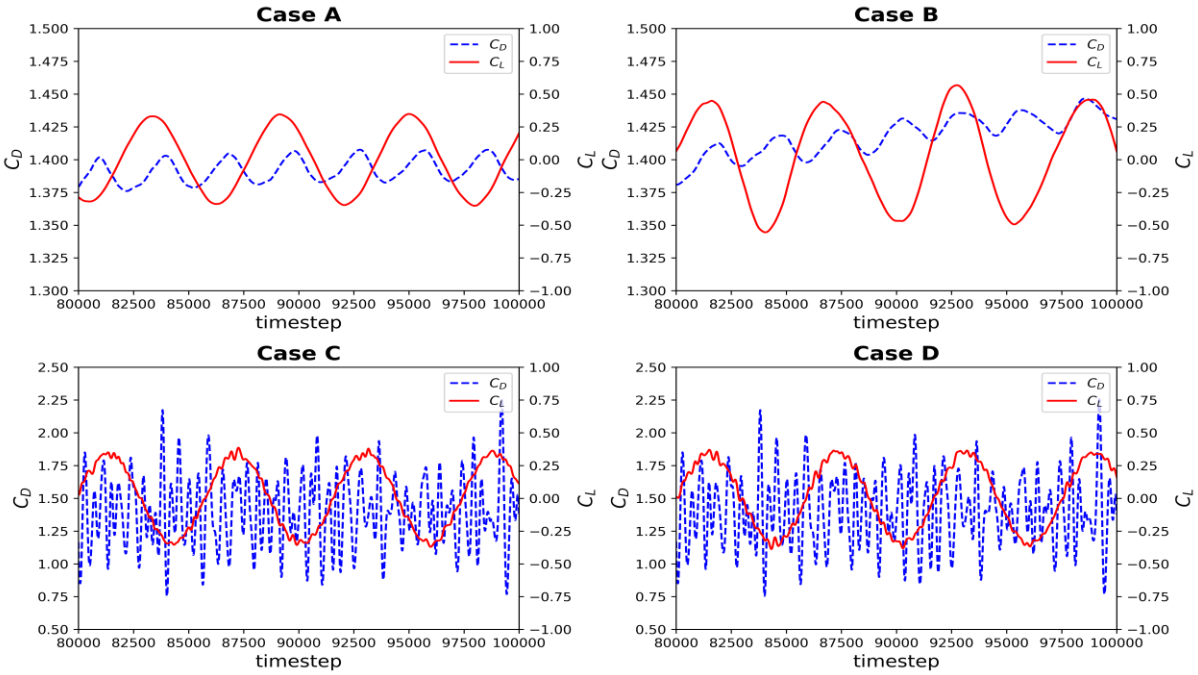

Figure 6. Temporal progression and comparison of the oscillation of the drag and lift coefficients for $Re = 100$.

Comparisons were made with several authors in the literature who used different solutions for the flow simulation. Figure 7 presents a comparison with the experimental data of Tritton (Tritton, 1959), showing a very good agreement for the drag coefficient in this range of the Reynolds number.

Comparisons were also made with other authors using different numerical procedures such as classical CFD, finite differences or finite volumes (Dennis; Chang, 1970; Fornberg, 1980; Park; Kwon; Choi, 1998; Sucker; Brauer, 1975) and with authors using the lattice Boltzmann method LBM (He; Doolen, 1997; Pellerin; Leclaire; Reggio, 2017; Surmas; Dos Santos; Philippi, 2004). These comparisons are presented in Tab. 4.

6. CONCLUSION

In this paper, several models of the Lattice Boltzmann Method were performed to study the aerodynamic forces acting in an immersed solid body, and comparisons between a variety of boundary conditions were made. All proposed cases showed excellent agreement with the results found in the literature, both for the coefficients obtained in the simulation and for the flow representation. However, the ascribed pressure boundary condition (cases C and D) at the exit of the numerical domain exhibited a great amount of noisy, which is supposed to be caused by the presence of pressure waves within the domain. In addition, the need for longer simulation times is notable for case B to reach the fully developed flow state. Concluding then that case A presented the best behavior compared to the expected in the literature.

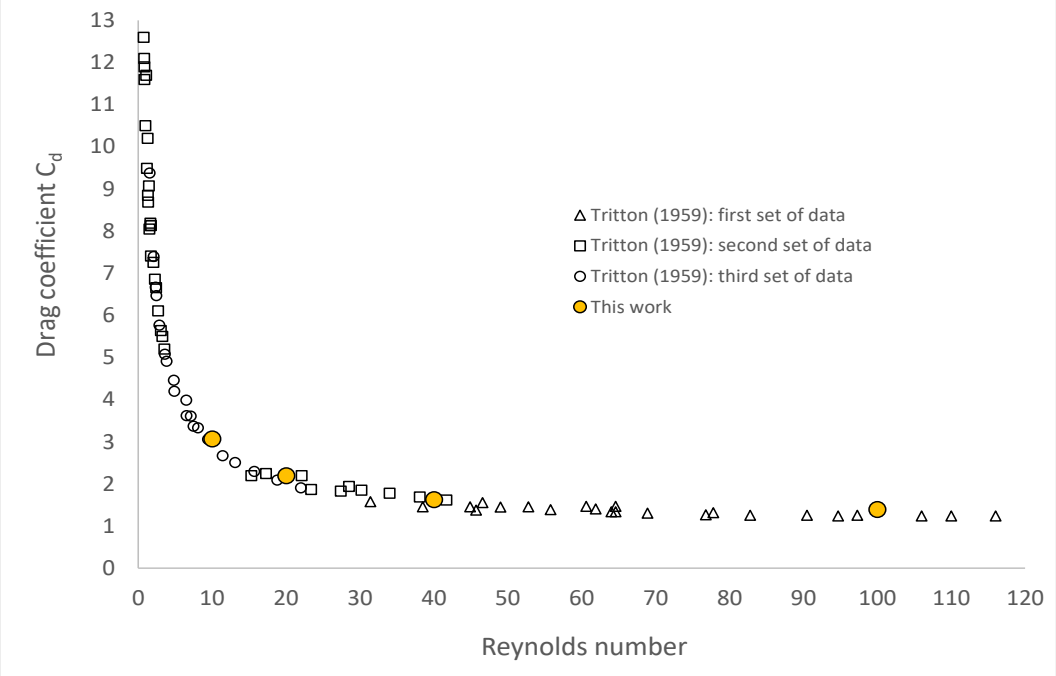

Figure 7. Comparison between the values for the drag coefficient obtained in this work and the experimental data of Tritton (1959).

Table 4. Comparison of the present simulation results for the drag coefficient with other authors.

		C_D			
	Re	10	20	40	100
CFD	Dennis & Chang (1970)	2.846	2.045	1.522	1.056
	Fornberg (1980)	-	2.000	1.498	1.058
	Park *et al.* (1998)	2.780	2.010	1.510	1.330
	Sucker and Brauer (1975)	2.831	2.178	1.633	1.243
LBM	He & Doolen (1997)	3.170	2.152	1.499	-
	Surmas *et al.* (2004)	2.800	2.000	1.500	1.400
	Pellerin *et al.* (2017)	-	2.003	1.502	1.326
	This work	3.072	2.195	1.631	1.398

7. REFERENCES

ABE, T. Derivation of the Lattice Boltzmann Method by Means of the Discrete Ordinate Method for the Boltzmann Equation. **Journal of Computational Physics**, v. 131, p. 241–246, 1997.

BHATNAGAR, P. L.; GROSS, E. P.; KROOK, M. A model for collision processes in gases. I. Small amplitude processes in charged and neutral one-component systems. **Physical Review**, v. 94, n. 3, 1954.

CHEN, S.; CHEN, H.; MARTÍNES, D.; MATTHAEUS, W. Lattice Boltzmann model for simulation of

magnetohydrodynamics. **Physical Review Letters**, v. 67, n. 27, p. 3776–3779, 1991.
CHEN, S.; DOOLEN, G. D. Lattice Boltzmann Method For Fluid Flows. **Annual Reviews of Fluid Mechanics**, v. 30, p. 329–364, 1998.
DENNIS, S. C. R.; CHANG, G. ZU. Numerical solutions for steady flow past a circular cylinder at Reynolds numbers up to 100. **Journal of Fluid Mechanics**, v. 42, p. 471–489, 1970.
FORNBERG, B. A numerical study of steady viscous flow past a circular cylinder. **Journal of Fluid Mechanics**, v. 98, p. 819–855, 1980.
GINZBURG, I.; VERHAEGHE, F.; D'HUMIÈRES, D. Two-relaxation-time Lattice Boltzmann scheme: About parametrization, velocity, pressure and mixed boundary conditions. **Communications in Computational Physics**, v. 3, n. 2, p. 427–478, 2008.
HE, X.; DOOLEN, G. D. Lattice Boltzmann Method on Curvilinear Coordinates System: Flow around a Circular Cylinder. **Journal of Computational Physics**, v. 134, p. 306–315, 1997.
HE, X.; LUO, L.-S. A priori derivation of the lattice Boltzmann equation. **Journal of Computational Physics**, v. 134, n. 2, 1997.
HEGELE, L. A. et al. High-Reynolds-number turbulent cavity flow using the lattice Boltzmann method. **Physical Review E**, v. 98, n. 4, p. 1–13, 2018.
HIGUERA, F. . J.; JIMÉNEZ, J. Boltzmann Approach to Lattice Gas Simulations. **Europhys. Lett.**, v. 9, n. 7, p. 663–668, 1989.
HIGUERA, F. . J.; SUCCI, S. Simulating the Flow Around a Circular Cylinder with a Lattice Boltzmann Equation. **Europhysics Letters**, v. 8, n. 6, p. 517–521, 1989.
KRUGER, T. et al. **The lattice boltzmann method: Principles and Practice**. [s.l.] Springer, 2017.
LUO, L. S. et al. Numerics of the lattice Boltzmann method: Effects of collision models on the lattice Boltzmann simulations. **Physical Review E - Statistical, Nonlinear, and Soft Matter Physics**, v. 83, n. 5, p. 1–24, 2011.
MATTILA, K. K.; PHILIPPI, P. C.; HEGELE, L. A. High-order regularization in lattice-Boltzmann equations. **Physics of Fluids**, v. 29, n. 4, 2017.
MCNAMARA, G. R.; ZANETTI, G. Use of the boltzmann equation to simulate lattice-gas automata. **Physical Review Letters**, v. 61, n. 20, 1988.
PARK, J.; KWON, K.; CHOI, H. Numerical solutions of flow past a circular cylinder at Reynolds numbers up to 160. **KSME International Journal**, v. 12, n. 6, p. 1200–1205, 1998.
PELLERIN, N.; LECLAIRE, S.; REGGIO, M. Solving incompressible fluid flows on unstructured meshes with the lattice boltzmann flux solver. **Engineering Applications of Computational Fluid Mechanics**, v. 11, n. 1, p. 310–327, 2017.
PHILIPPI, P. C.; HEGELE, L. A.; DOS SANTOS, L. O. E.; SURMAS, R. From the continuous to the lattice Boltzmann equation: The discretization problem and thermal models. **Physical Review E - Statistical, Nonlinear, and Soft Matter Physics**, v. 73, n. 5, p. 1–12, 2006.
PHILIPPI, P. C. **Lectures on the Lattice-Boltzmann Method given at the Graduate Program of Mechanical Engineering,**PUCPR, , 2018.
QIAN, Y. H.; D'HUMIÈRES, D.; LALLEMAND, P. Lattice BGK models for navier-stokes equation. **Europhys. Lett.**, v. 17, n. 6, p. 479–484, 1992.
ROTHMAN, D. H.; ZALESKI, S. **Lattice-gas cellular automata, simple models of complex hydrodynamics**. Cambridge, UK: University of Cambridge, 1997.
SHAN, X.; YUAN, X. F.; CHEN, H. Kinetic theory representation of hydrodynamics: A way beyond the Navier-Stokes equation. **Journal of Fluid Mechanics**, v. 550, p. 413–441, 2006.
SUCCI, S. **The Lattice Boltzmann Equation for Fluid Dynamics and Beyond**. [s.l.] Oxford University Press, 2001.
SUCKER, D.; BRAUER, H. Fluiddynamik bei quer angestromten Zylindern. **Warme und Stoffubertragung**, v. 8, n. 3, p. 149–158, 1975.
SURMAS, R.; DOS SANTOS, L. O. E.; PHILIPPI, P. C. Lattice Boltzmann simulation of the flow interference in bluff body wakes. **Future Generation Computer Systems**, v. 20, p. 951–958, 2004.
TRITTON, D. J. Experiments on the flow past a circular cylinder at low Reynolds numbers. **Journal of Fluid Mechanics**, v. 6, n. 4, p. 547–567, 1959.
ZHANG, R.; SHAN, X.; CHEN, H. Efficient kinetic method for fluid simulation beyond the Navier-Stokes equation. **Physical Review E - Statistical, Nonlinear, and Soft Matter Physics**, v. 74, n. 4, p. 1–7, 2006.
ZOU, Q.; HE, X. On pressure and velocity flow boundary conditions and bounceback for the lattice Boltzmann BGK model. **Physics of Fluids**, v. 9, n. 1591, 1997.

8. RESPONSIBILITY NOTICE

The authors are the only responsible for the printed material included in this paper.